Ternary Stannides $RE_3Ru_4Sn_{13}$ (RE = La, Ce, Pr, Nd) – Structure, Magnetic Properties, and ^{119}Sn Mössbauer Spectroscopy

Trinath Mishra, Christian Schwickert, Thorsten Langer, and Rainer Pöttgen

Institut für Anorganische und Analytische Chemie, Universität Münster, Corrensstraße 30, 48149 Münster, Germany

Reprint requests to R. Pöttgen. E-mail: pottgen@uni-muenster.de

Z. Naturforsch. **2011**, *66b,* 664 – 670; received June 8, 2011

The ternary stannides $RE_3Ru_4Sn_{13}$ (RE = La, Ce, Pr, Nd) were obtained by arc-melting of the elements. The polycrystalline samples were characterized by powder X-ray diffraction. The structures of three compounds were refined from single-crystal diffractometer data: $Yb_3Rh_4Sn_{13}$ type, $Pm\bar{3}n$, a = 977.74(3) pm, $wR2$ = 0.0379, 280 F^2 values for $La_3Ru_4Sn_{13}$, a = 971.34(9) pm, $wR2$ = 0.0333, 274 F^2 values for $Ce_3Ru_4Sn_{13}$, a = 970.68(8) pm, $wR2$ = 0.0262, 272 F^2 values for $Nd_3Ru_4Sn_{13}$ with 13 variables per refinement. The structures consist of three-dimensional networks of condensed $RuSn_{6/2}$ trigonal prisms with the RE (CN 16) and Sn2 (CN 12) atoms in two different types of cavities of the networks. The two crystallographically independent tin sites have been resolved by ^{119}Sn Mössbauer spectroscopy. Temperature-dependent magnetic susceptibility measurements of $Ce_3Ru_4Sn_{13}$ gave a reduced magnetic moment of 2.32 μ_B per Ce atom, indicating intermediate cerium valence. No magnetic ordering was evident down to 3 K.

Key words: Intermetallics, Rare Earth Compounds, Stannide, Crystal Structure

Introduction

Filled skutterudites RET_4Pn_{12} (RE = rare earth element, T = transition metal; Pn = pnictide) have been in the focus of solid-state research for thirty years. They exhibt highly interesting physical properties such as ferromagnetism, superconductivity, Kondo insulator or non-Fermi liquid behavior, or heavy-fermion states. Most of the recent systematic research on such skutterudites focused on their excellent thermoelectric properties. For an overview we refer to a review article by Sales [1]. The use of the materials for thermoelectric applications is directly related to a structural peculiarity. The rare earth atoms fill larger cages (Wyckoff site 2*a*) within a network of condensed, tilted $TPn_{6/2}$ octahedra and show enhanced displacement parameters (*rattling* of the rare earth atoms) which strongly reduces the thermal conductivity.

Similar structural features occur in the structure types $LaRuSn_3$ [2] and $Yb_3Rh_4Sn_{13}$ [3]. The two structure types, space groups $Pm\bar{3}n$, just differ in the occupancy of the 2*a* Wyckoff sites, *i. e.* rare earth atoms in the $LaRuSn_3$ but tin atoms in the $Yb_3Rh_4Sn_{13}$ type. The transition metal atoms have trigonal prismatic tin coordination and one observes a three-dimensional network of condensed, tilted $TSn_{6/2}$ trigonal prisms. As an example we present the structures of $LaFe_4P_{12}$ [4], $LaRuSn_3$ [2] and $La_3Ru_4Sn_{13}$ (described herein) in Fig. 1. The *rattling* of the rare earth atoms in the networks of condensed trigonal prisms has first been described for the series of REPtIn$_3$ (RE = La, Ce, Pr, Nd, Sm) indides [5]. Initially the $RE_3T_4Sn_{13}$ stannides have intensively been studied with respect to their superconducting behavior [6, 7]. Later on, the RERuSn$_3$ stannides and various compositions RERuSn$_x$ ($2.85 \leq x \leq 3.15$) have been investigated with regard to the heavy fermion ground state of $CeRuSn_3$ and the valence fluctuation in $SmRuSn_3$ [8 – 14].

The composition of the samples has been studied by two groups. Fukuhara *et al.* [11] mentioned crystal growth experiments of $Ce_3Ru_4Sn_{13}$, however, their X-ray diffraction patterns showed considerable amounts of Ru_3Sn_7 as a by-product. The assignment of composition $LaRuSn_3$ was based on chemical analysis (atomic absorption spectroscopy for La and Sn; Ru just as the difference) [2]. Phase analytical work on the Nd-Ru-Sn system by Salamakha *et al.* [15] showed the formation of a solid solution $Nd_{3+x}Ru_4Sn_{13-x}$, including both compositions as border phases.

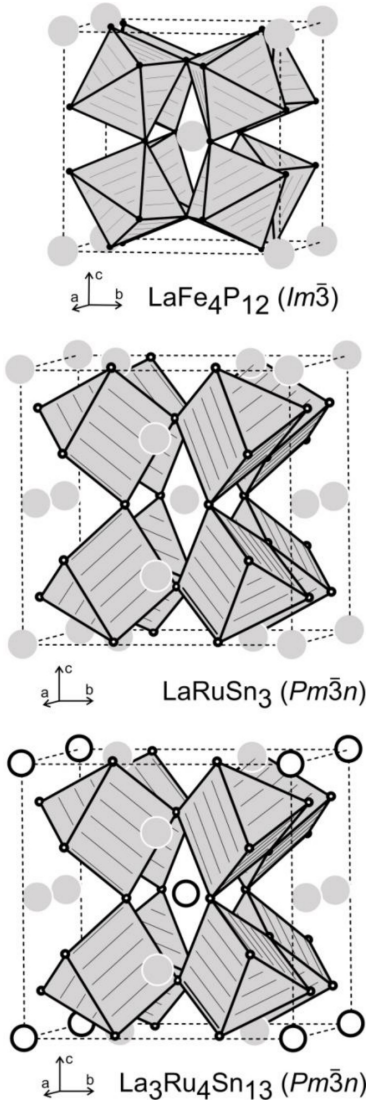

Fig. 1. The structures of $LaFe_4P_{12}$, $LaRuSn_3$, and $La_3Ru_4Sn_{13}$. Lanthanum, iron (ruthenium), and phosphorus (tin) atoms are drawn as medium grey, black filled, and open circles, respectively. The networks of condensed $FeP_{6/2}$ octahedra and $RuSn_{6/2}$ trigonal prisms are emphasized.

In the course of our systematic research on intermediate-valent or mixed-valent $Ce_xRu_yX_z$ (X = element of the 3rd or 4th main group, Mg, Cd) compounds [16 – 20, and refs. therein] we have reinvestigated the structure of $Ce_3Ru_4Sn_{13}$ and the members with RE = La, Pr, and Nd. Herein we report high-quality single-crystal data, complemented by a characterization of $Ce_3Ru_4Sn_{13}$ by ^{119}Sn Mössbauer spectroscopy and magnetic susceptibility measurements.

Table 1. Lattice parameters of the $RE_3Ru_4Sn_{13}$ (RE = La, Ce, Pr, Nd) compounds.

Compound	a (pm)	V (nm^3)	Ref.
$La_3Ru_4Sn_{13}$	977.2	0.9332	[6, 7]
$La_3Ru_4Sn_{13}$	977.74(3)	0.9347	this work
$LaRuSn_3$	977.3(5)	0.9334	[2]
$LaRuSn_3$	977	0.9326	[8]
$Ce_3Ru_4Sn_{13}$	972.4	0.9195	[7]
$Ce_3Ru_4Sn_{13}$	971.34(9)	0.9165	this work
$CeRuSn_3$	972.6(5)	0.9200	[2]
$CeRuSn_3$	973	0.9212	[8]
$Pr_3Ru_4Sn_{13}$	971.2	0.9161	[7]
$Pr_3Ru_4Sn_{13}$	970.85(4)	0.9151	this work
$PrRuSn_3$	970.8(5)	0.9149	[2]
$Nd_3Ru_4Sn_{13}$	970.7	0.9147	[7]
$Nd_3Ru_4Sn_{13}$	970.68(8)	0.9146	this work
$NdRuSn_3$	968.7(5)	0.9090	[2]

Experimental Section

Synthesis

Starting materials for the preparation of the $RE_3Ru_4Sn_{13}$ samples were ingots of the rare earth metals (Johnson Matthey or smart elements), ruthenium powder (Degussa-Hüls, *ca.* 200 mesh), and tin granules (Merck). In the first step, pieces of the rare earth ingots were arc-melted [21] under argon (*ca.* 700 mbar) to small buttons. The argon was purified before with titanium sponge (870 K), silica gel and molecular sieves. The moisture-sensitive rare earth buttons were kept in Schlenk tubes prior to the reactions. The elements were then weighed in the ideal 3 : 4 : 13 atomic ratio (the ruthenium powder was cold-pressed to a pellet of 6 mm diameter) and arc-melted. The molten product buttons were remelted three times to ensure homogeneity. The total weight loss after the melting procedures was less than 0.5 %. The polycrystalline $RE_3Ru_4Sn_{13}$ samples are stable in air for months. Single crystals exhibit metallic luster while ground powder is dark grey.

EDX data

Semiquantitative EDX analyses on the crystals investigated on the diffractometer were carried out by use of a Zeiss EVO® MA10 scanning electron microscope in variable pressure mode with LaB_6, CeO_2, NdF_3, Ru, and Sn as standards. The experimentally observed compositions (17 at.-% La : 21 at.-% Ru : 62 at.-% Sn; 18 at.-% Ce : 21 at.-% Ru : 61 at.-% Sn; 15 at.-% Nd : 22 at.-% Ru : 63 at.-% Sn) were close to the ideal one (15 : 20 : 65). No impurity elements have been found.

X-Ray diffraction

The purity of the polycrystalline $RE_3Ru_4Sn_{13}$ samples was checked by Guinier powder patterns (imaging plate detector, Fujifilm BAS-1800 readout system) with Cu$K_{\alpha1}$ ra-

Table 2. Crystallographic data and structure refinements for $RE_3Ru_4Sn_{13}$ (*RE* = La, Ce, Nd), $Yb_3Rh_4Sn_{13}$ type, space group $Pm\bar{3}n$, $Z = 2$.

Empirical formula	$La_3Ru_4Sn_{13}$	$Ce_3Ru_4Sn_{13}$	$Nd_3Ru_4Sn_{13}$
Molar mass, g mol^{-1}	2363.98	2367.61	2379.97
Lattice parameters	Table 1	Table 1	Table 1
Crystal size, μm^3	$20 \times 30 \times 40$	$20 \times 35 \times 50$	$20 \times 40 \times 60$
Calculated density, g cm^{-3}	8.40	8.58	8.64
Transm. ratio, max / min	0.766 / 0.659	0.735 / 0.611	0.758 / 0.597
Radiation	MoK_α	MoK_α	MoK_α
λ, pm	71.073	71.073	71.073
Absorption coeff., mm^{-1}	26.8	27.8	28.9
F(000), e	1994	2000	2012
θ-range, deg.	3 – 31	3 – 31	3 – 31
Range in *hkl*	$\pm$13, $\pm$13, $\pm$13	$\pm$13, $\pm$13, $\pm$13	$\pm$13, $\pm$13, $\pm$13
Total no. reflections	9102	9132	9417
Independent reflections / $R_{\rm int}$	280 / 0.0918	274 / 0.0762	272 / 0.0521
Reflections with $I \geq 2\sigma(I)$ / R_σ	251 / 0.0285	264 / 0.0223	250 / 0.0166
Data / ref. parameters	280 / 13	274 / 13	272 / 13
Goodness-of-fit on F^2	1.211	1.371	1.241
$R1$ / $wR2$ for $I \geq 2\sigma(I)$	0.0258 / 0.0360	0.0242 / 0.0329	0.0233 / 0.0252
$R1$ / $wR2$ for all data	0.0351 / 0.0379	0.0274 / 0.0333	0.0301 / 0.0262
Extinction coefficient	0.0015(1)	0.0017(1)	0.00035(4)
Largest diff. peak / hole, e Å^{-3}	1.46 / −0.96	1.00 / −0.93	1.05 / −1.16

Table 3. Atomic coordinates and isotropic displacement parameters (pm^2) for $RE_3Ru_4Sn_{13}$ (*RE* = La, Ce, Nd). $U_{\rm eq}$ is defined as one third of the trace of the orthogonalized $U_{\rm ij}$ tensor.

Atom	Wyckoff site	*x*	*y*	*z*	U_{11}	U_{22}	U_{33}	U_{23}	U_{13}	U_{12}	$U_{\rm eq}$
$La_3Ru_4Sn_{13}$											
La	6*c*	1/2	1/4	0	75(2)	83(3)	U_{11}	0	0	0	78(2)
Ru	8*e*	1/4	1/4	1/4	59(2)	U_{11}	U_{11}	5(2)	U_{23}	U_{23}	59(2)
Sn1	24*k*	0.15587(5)	0.30635(6)	0	83(2)	278(3)	51(2)	0	0	48(2)	137(2)
Sn2	2*a*	0	0	0	294(5)	U_{11}	U_{11}	0	0	0	294(5)
$Ce_3Ru_4Sn_{13}$											
Ce	6*c*	1/2	1/4	0	71(2)	83(3)	U_{11}	0	0	0	75(2)
Ru	8*e*	1/4	1/4	1/4	53(2)	U_{11}	U_{11}	6(1)	U_{23}	U_{23}	53(2)
Sn1	24*k*	0.15539(4)	0.30713(5)	0	74(2)	249(2)	49(2)	0	0	40(1)	124(1)
Sn2	2*a*	0	0	0	279(4)	U_{11}	U_{11}	0	0	0	279(4)
$Nd_3Ru_4Sn_{13}$											
Nd	6*c*	1/2	1/4	0	86(2)	101(3)	U_{11}	0	0	0	91(1)
Ru	8*e*	1/4	1/4	1/4	64(1)	U_{11}	U_{11}	4(1)	U_{23}	U_{23}	64(1)
Sn1	24*k*	0.15499(4)	0.30569(5)	0	84(2)	221(2)	59(2)	0	0	29(2)	121(1)
Sn2	2*a*	0	0	0	255(4)	U_{11}	U_{11}	0	0	0	255(4)

diation and α-quartz (a = 491.30 and c = 540.46 pm) as the internal standard. The cubic lattice parameters (Table 1) were obtained through least-squares refinements. The experimental patterns were compared to calculated ones [22] to ensure correct indexing.

Small irregular single crystal fragments of the stannides $RE_3Ru_4Sn_{13}$ (*RE* = La, Ce, Nd) were separated from the crushed samples. They were glued to quartz fibers using bees wax and first investigated on a Buerger precession camera (white Mo radiation, Fuji-film imaging plate) in order to check the quality for intensity data collection. The data sets were collected at r. t. by use of a Stoe IPDS-II image plate system (graphite-monochromatized MoK_α radiation; λ = 71.073 pm) in oscillation mode. Numerical absorption corrections were applied to the data. Details on the crystallographic data are given in Table 2.

Structure refinements

The three diffractometer data sets showed primitive cubic lattices, and the extinction conditions were compatible with space group $Pm\bar{3}n$, in agreement with our previous results on $Ce_3Rh_4Sn_{13}$ and $Ce_3Ir_4Sn_{13}$ [23]. The atomic parameters of $Ce_3Rh_4Sn_{13}$ were taken as starting values, and the structures were refined using SHELXL-97 [24] (full-matrix least-squares on F^2) with anisotropic atomic displacement parameters for all sites. Since there were contradictory reports on the compositions of these phases (1-1-3 ≡ 4-4-12

Table 4. Interatomic distances (pm) in the structures of $RE_3Ru_4Sn_{13}$ (*RE* = La, Ce, Nd). All distances within the first coordination shells are listed. Standard deviations are all equal or smaller than 0.1 pm.

			$La_3Ru_4Sn_{13}$	$Ce_3Ru_4Sn_{13}$	$Nd_3Ru_4Sn_{13}$
RE:	4	Sn1	340.9	339.3	339.2
	8	Sn1	344.7	341.8	342.2
	4	Ru	345.7	343.4	343.2
	2	*RE*	488.9	485.7	485.3
Ru:	6	Sn1	266.9	265.5	265.2
	3	*RE*	345.7	343.4	343.2
Sn1:	2	Ru	266.9	265.5	265.2
	1	Sn1	304.8	301.9	300.9
	2	Sn1	324.9	322.5	324.3
	1	Sn2	336.1	334.3	332.7
	1	*RE*	340.9	339.3	339.2
	2	*RE*	344.7	341.8	342.2
Sn2:	12	Sn1	336.1	334.3	332.7

vs. 3-4-13) and since the Sn2 sites even showed defects in $Ce_3Rh_4Sn_{13}$ and $Ce_3Ir_4Sn_{13}$ [23], we refined the occupancy parameters in separate series of least-squares cycles. For all three crystals, all sites were fully occupied within one standard deviation. This is consistent with the starting compositions, the phase-pure powder diagrams and the ^{119}Sn Mössbauer spectroscopic data (*vide infra*). As a test run we refined the 2*a* site of the lanthanum-based crystal with the scattering power of lanthanum, resulting in an occupancy of only 89(1) %, clearly not consistent with all other data. The final difference Fourier syntheses were flat. The refined positional parameters and interatomic distances are listed in Tables 3 and 4.

Further details on the structure refinements may be obtained from Fachinformationszentrum Karlsruhe, 76344 Eggenstein-Leopoldshafen, Germany (fax: +49-7247-808-666; e-mail: crysdata@fiz-karlsruhe.de, http://www.fiz-informationsdienste.de/en/DB/icsd/depot_anforderung.html) on quoting the deposition number CSD-423134 ($La_3Ru_4Sn_{13}$), CSD-423135 ($Ce_3Ru_4Sn_{13}$), and CSD-423136 ($Nd_3Ru_4Sn_{13}$).

^{119}*Sn Mössbauer spectroscopy*

A $Ca^{119m}SnO_3$ source was available for the ^{119}Sn Mössbauer spectroscopic investigations. $Ce_3Ru_4Sn_{13}$ and β-Sn samples were placed within thin-walled PMMA containers at a thickness of about 10 mg Sn cm^{-2}. A palladium foil of 0.05 mm thickness was used to reduce the tin K X-rays concurrently emitted by this source. The measurements were conducted in the usual transmission geometry at 77 K.

Magnetic measurements

The magnetic measurement of the $Ce_3Ru_4Sn_{13}$ sample was carried out on a Quantum Design Physical Property Measurement System (PPMS) using the VSM option. The sample (24.173 mg) was packed in kapton foil and attached to the sample holder rod for measuring the magnetic properties in the temperature range 3 – 300 K with magnetic flux densities up to 80 kOe.

Discussion

Crystal chemistry

The present single-crystal structure refinements of $La_3Ru_4Sn_{13}$, $Ce_3Ru_4Sn_{13}$, and $Nd_3Ru_4Sn_{13}$ clearly revealed that besides the RERuSn$_3$ series (*i. e.* 4-4-12), another series of 3-4-13 compounds also exists. Herein, when quoting interatomic distances, we exemplarily discuss the $Ce_3Ru_4Sn_{13}$ structure. The unit cell is presented in Fig. 1. The ruthenium atoms have trigonal prismatic tin coordination at Ru–Sn1 distances of 266 pm, close to the sum of the covalent radii [25] of 264 pm. We can therefore assume essentially covalent Ru–Sn bonding. The $RuSn_{6/2}$ trigonal prisms are condensed *via* common corners leading to the three-dimensional network emphasized in Fig. 1. In the structure of $CeRu_4Sn_6$ [26] the monomeric units of the [Ru_4Sn_6] network are strongly distorted $RuSn_{6/4}$ octahedra with a similar range of Ru–Sn distances (257 – 277 pm). A slightly broader range of Ru–Sn distances was observed in the complex polyanionic [RuSn] network of CeRuSn (265 – 290 pm) [16].

The three-dimensional network of condensed prisms leaves two different kinds of cavities which are filled by the cerium (Wyckoff site 6*c*) and Sn2 (Wyckoff site 2*a*) atoms. The larger cerium atoms have coordination number 16 (12 Sn + 4 Rh), and the Sn2 atoms have CN 12 by Sn1 atoms in icosahedral arrangement. The Sn2 atoms within the Sn1 icosahedra show full occupancy, but strongly enhanced displacement parameters, indicating a *rattling* within the icosahedral voids. The Sn1 atoms surrounding Sn2 react on this rattling and show enhanced U_{22} parameters. These structural features are similar to those of the skutterudites and have been discussed in detail in an earlier work on $LaPtIn_3$ [5].

The Sn–Sn distances in the $Ce_3Ru_4Sn_{13}$ structure range from 302 to 334 pm. They compare well with the structure of β-Sn (4×302 and 2×318 pm) [27]. From Table 4 it is evident that the Sn2 atoms with the higher coordination number also have the longer distances. The polyhedra of the two different tin sites, Sn1 with CN 9 and Sn2 with CN 12, are presented in Fig. 2. Due to the irregular coordination, the Sn1 atoms have

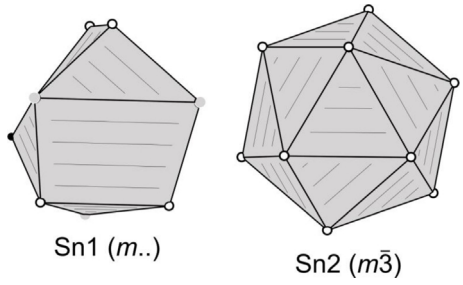

Fig. 2. Coordination of the two crystallographically independent tin atoms in $La_3Ru_4Sn_{13}$. Lanthanum, ruthenium, and tin atoms are drawn as medium grey, black filled and open circles, respectively. The site symmetries are indicated.

low site symmetry *m*.., while the icosahedrally coordinated Sn2 atoms have site symmetry $m\bar{3}$. We draw back to these site symmetries in the following chapter on ^{119}Sn Mössbauer spectroscopy.

Finally we comment on the course of the lattice parameters (Table 1) and the course of the interatomic distances (Table 4) in going from $La_3Ru_4Sn_{13}$ *via* $Ce_3Ru_4Sn_{13}$ to $Nd_3Ru_4Sn_{13}$. The cerium compound shows a slight negative anomaly in the Iandelli plot [11], indicating a tendency towards intermediate cerium valence. This is also manifested by the interatomic distances of the cerium atoms which are similar or even slightly smaller than those of the neodymium compound.

^{119}*Sn Mössbauer spectroscopy*

The experimental and simulated ^{119}Sn Mössbauer spectra of $Ce_3Ru_4Sn_{13}$ and β-Sn samples at 77 K are presented in Fig. 3. The spectrum of $Ce_3Ru_4Sn_{13}$ consists of two sub-spectra. The Sn1 atoms (Wyckoff site 24*k* with site symmetry *m*..) show an isomer shift of δ = 2.15(1) mm s^{-1} and substantial quadrupole splitting of ΔE_Q = 1.90(1) mm s^{-1}, in agreement with the highly asymmetric Sn1 coordination (Fig. 2). The experimental line width amounts to Γ = 1.13(2) mm s^{-1}. This quadrupole-split subspectrum is superimposed on a singlet of the Sn2 atoms (Wyckoff site 2*a* with site symmetry $m\bar{3}$) with the fitting parameters δ = 2.62(5) mm s^{-1} and Γ = 0.9(2) mm s^{-1}. Due to the cubic site symmetry, no quadrupole splitting is observed for this signal. The refined intensity ratio of both signals of 90(1) : 10(1) is in good agreement with the ideal value of 92.3 : 7.7. This result indicates a similar situation as in isotypic $Ce_3Rh_4Sn_{13}$ [23].

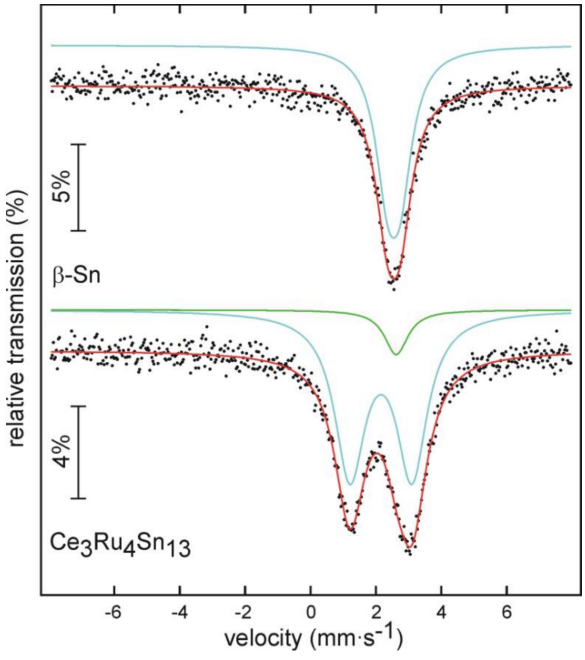

Fig. 3. Experimental and simulated ^{119}Sn Mössbauer spectrum of β-Sn and $Ce_3Ru_4Sn_{13}$ at 77 K.

The electronic situation of the two tin sites in $Ce_3Ru_4Sn_{13}$ is slightly different. The Sn2 atoms within the $Sn1_{12}$ icosahedra show a slightly higher isomer shift, indicating a slightly higher electron density at the Sn2 nuclei. For comparison we have plotted the spectrum of β-Sn (flattended $SnSn_4$ tetrahedra) in the same Figure. Refinement of the spectrum led to δ = 2.55(1) mm s^{-1} and ΔE_Q = 0.40(2) mm s^{-1}, in good agreement with literature data [28]. This nicely underlines the metallic nature of Sn2 within the $Sn1_{12}$ icosahedra.

Magnetic properties

The temperature dependence of the magnetic susceptibility [$\chi(T)$ and $\chi^{-1}(T)$ data] of $Ce_3Ru_4Sn_{13}$ measured in a field of 10 kOe is shown in Fig. 4. In the temperature range of 20 – 300 K we were able to fit $\chi^{-1}(T)$ data using a modified Curie-Weiss law, leading to a temperature-independent term χ_0 = 1.96×10^{-3} emu mol^{-1}, an effective magnetic moment of 2.32(1) μ_B per Ce atom, and a Weiss constant of θ = −16.1(5) K. Variation of the fitting range to the higher temperature regime did only marginally change the fitting parameters (χ_0 = 1.51×10^{-3} emu mol^{-1}, 2.39(1) μ_B per Ce atom, θ = −19.1(5) K for the 100 –

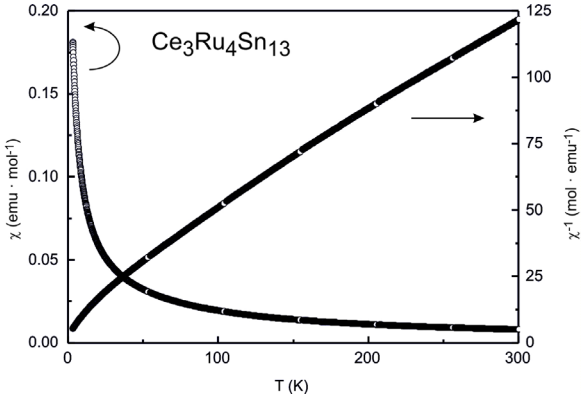

Fig. 4. Temperature dependence of the magnetic susceptibility (χ and χ^{-1} data) of $Ce_3Ru_4Sn_{13}$ measured at 10 kOe.

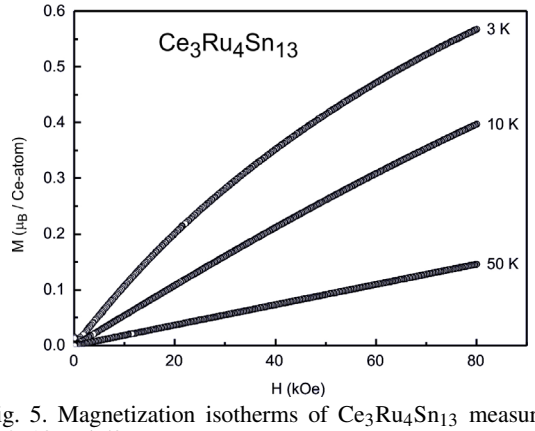

Fig. 5. Magnetization isotherms of $Ce_3Ru_4Sn_{13}$ measured at 3, 10 and 50 K.

300 K range). The experimentally determined moment is smaller than the theoretical value of 2.54 μ_B for a free Ce^{3+} ion, indicating that only approximately 83 % of the cerium atoms are in a trivalent state. If one assumes the composition $CeRuSn_3$ for our sample, a strongly reduced moment of 2.02 μ_B per Ce atom results. This would not be in line with the original reports [8, 9, 11] and clearly confirms the composition $Ce_3Ru_4Sn_{13}$.

Fig. 5 displays the magnetization isotherms of $Ce_3Ru_4Sn_{13}$ measured at 3, 10 and 50 K, with an applied external field between 0 and 80 kOe. A field-induced increase of the magnetization is observed at 3 K. The 10 K magnetization isotherm is slightly curved, and at 50 K we observe a linear dependence of the magnetization from the applied external field as expected for a paramagnetic material. The saturation magnetization of 0.57(1) μ_B per Ce atom at 3 K and 80 kOe is lower than the theoretical value of 2.14 μ_B per Ce atom according to $g_J \times J$.

Acknowledgements

This work was financially supported by the Deutsche Forschungsgemeinschaft. T. M. is indebted to the Forschungsschule *Molecules and Materials – A Common Design Principle* for a PhD stipend.

[1] B. C. Sales, Filled Skutterudites, in K. A. Gschneidner, Jr., J.-C. G. Bünzli, V. K. Pecharsky, *Handbook on the Physics and Chemistry of Rare Earths*, Elsevier Science, Vol. 33, **2003**, chapter 211, pp. 1.
[2] B. Eisenmann, H. Schäfer, *J. Less-Common Met.* **1986**, *123*, 89.
[3] J. L. Hodeau, J. Chenavas, M. Marezio, J. P. Remeika, *Solid State Commun.* **1980**, *36*, 839.
[4] W. Jeitschko, D. Braun, *Acta Crystallogr.* **1977**, *B33*, 3401.
[5] Y. V. Galadzhun, R. Pöttgen, *Z. Anorg. Allg. Chem.* **1999**, *625*, 481.
[6] G. P. Espinosa, A. S. Cooper, H. Barz, J. P. Remeika, *Mater. Res. Bull.* **1980**, *15*, 1635.
[7] G. P. Espinosa, A. S. Cooper, H. Barz, *Mater. Res. Bull.* **1982**, *17*, 963.
[8] T. Fukuhara, I. Sakamoto, H. Sato, S. Takayanagi, N. Wada, *J. Phys.: Condens. Matter* **1989**, *1*, 7487.
[9] S. Takayanagi, T. Fukuhara, H. Sato, N. Wada, Y. Yamada, *Physica B* **1990**, *165&166*, 447.
[10] S. Takayanagi, T. Fukuhara, H. Sato, N. Wada, *Physica C* **1991**, *185 – 189*, 2643.
[11] T. Fukuhara, I. Sakamoto, H. Sato, *J. Phys.: Condens. Matter* **1991**, *3*, 8917.
[12] T. Fukuhara, S. Iwakawa, H. Sato, *J. Magn. Magn. Mater.* **1992**, *104 – 107*, 667.
[13] H. Ishii, T. Hanyu, T. Fukuhara, I. Sakamoto, H. Sato, S. Yamaguchi, *J. Phys. Soc. Jpn.* **1993**, *62*, 811.
[14] C. Godart, C. Mazumdar, S. K. Dhar, R. Nagarajan, L. C. Gupta, B. D. Padalia, R. Vijayaraghavan, *Phys. Rev. B* **1993**, *48*, 16402.
[15] P. Salamakha, P. Demchenko, J. Stępień-Damm, *J. Alloys Compd.* **1997**, *260*, L1.
[16] J. F. Riecken, W. Hermes, B. Chevalier, R.-D. Hoffmann, F. M. Schappacher, R. Pöttgen, *Z. Anorg. Allg. Chem.* **2007**, *633*, 1094.

[17] S. F. Matar, J. F. Riecken, B. Chevalier, R. Pöttgen, V. Eyert, *Phys. Rev. B* **2007**, *76*, 174434.
[18] R. Mishra, W. Hermes, U. Ch. Rodewald, R.-D. Hoffmann, R. Pöttgen, *Z. Anorg. Allg. Chem*. **2008**, *634*, 470.
[19] W. Hermes, S. F. Matar, R. Pöttgen, *Z. Naturforsch*. **2009**, *64b*, 901.
[20] S. Linsinger, M. Eul, U. Ch. Rodewald, R. Pöttgen, *Z. Naturforsch*. **2010**, *65b*, 1185.
[21] R. Pöttgen, Th. Gulden, A. Simon, *GIT Labor-Fachzeitschrift* **1999**, *43*, 133.
[22] K. Yvon, W. Jeitschko, E. Parthé, *J. Appl. Crystallogr.* **1977**, *10*, 73.
[23] D. Niepmann, R. Pöttgen, K. M. Poduska, F. J. DiSalvo, H. Trill, B. D. Mosel, *Z. Naturforsch*. **2001**, *56b*, 1.
[24] G. M. Sheldrick, SHELXL-97, Program for the Refinement of Crystal Structures, University of Göttingen, Göttingen (Germany) **1997**. See also: G. M. Sheldrick, *Acta Crystallogr.* **2008**, *A64*, 112.
[25] J. Emsley, *The Elements*, Oxford University Press, Oxford **1999**.
[26] R. Pöttgen, R.-D. Hoffmann, E. V. Sampathkumaran, I. Das, B. D. Mosel, R. Müllmann, *J. Solid State Chem*. **1997**, *134*, 326
[27] J. Donohue, *The Structures of the Elements*, Wiley, New York, **1974**.
[28] P. E. Lippens, *Phys. Rev. B* **1999**, *60*, 4576.